

Improving the Output Efficiency of Triboelectric Nanogenerator by a Power Regulation Circuit

Wenbo Li ^{1,2}, Baichuan Leng ¹, Shengyu Hu ¹ and Xiaojun Cheng ^{1,2,*}

¹ Beijing Institute of Nanoenergy and Nanosystems, Chinese Academy of Sciences, Beijing 101400, China; liwenbo@binn.cas.cn (W.L.); lengbaichuan@binn.cas.cn (B.L.); hushengyu@binn.cas.cn (S.H.)

² School of Nanoscience and Technology, University of Chinese Academy of Sciences, Beijing 100049, China

* Correspondence: chengxiaojun@binn.cas.cn

Abstract: Triboelectric nanogenerator (TENG) is a promising technology for harvesting energy from various sources, such as human motion, wind and vibration. At the same time, a matching backend management circuit is essential to improve the energy utilization efficiency of TENG. Therefore, this work proposes a power regulation circuit (PRC) suitable for TENG, which is composed of a valley-filling circuit and a switching step-down circuit. The experimental results indicate that after incorporating a PRC, the conduction time of each cycle of the rectifier circuit doubles, increasing the number of current pulses in the TENG output and resulting in an output charge that is 1.6 fold that of the original circuit. Compared with the initial output signal, the charging rate of the output capacitor increased significantly by 75% with a PRC at a rotational speed of 120 rpm, significantly improving the utilization efficiency of the TENG's output energy. At the same time, when the TENG powers LEDs, the flickering frequency of LEDs is reduced after adding a PRC, and the light emission is more stable, which further verifies the test results. The PRC proposed in this study can enable the energy harvested by the TENG to be utilized more efficiently, which has a certain promoting effect on the development and application of TENG technology.

Keywords: triboelectric nanogenerator; power regulation circuit; performance improvement; conduction time; two-stage output



Citation: Li, W.; Leng, B.; Hu, S.; Cheng, X. Improving the Output Efficiency of Triboelectric Nanogenerator by a Power Regulation Circuit. *Sensors* **2023**, *23*, 4912. <https://doi.org/10.3390/s23104912>

Academic Editors: KC Aw, Junlei Wang, Mengying Xie, Wee Chee Gan and Hailing Fu

Received: 14 April 2023

Revised: 8 May 2023

Accepted: 17 May 2023

Published: 19 May 2023



Copyright: © 2023 by the authors. Licensee MDPI, Basel, Switzerland. This article is an open access article distributed under the terms and conditions of the Creative Commons Attribution (CC BY) license (<https://creativecommons.org/licenses/by/4.0/>).

1. Introduction

Energy is an indispensable factor for social development. With the increasing severity of the energy crisis and the increasing requirements for environmental protection, the demand for sustainable and efficient energy conversion and storage technologies is becoming more and more urgent [1–3]. In recent years, the innovation of new energy and the utilization of environmental energy have been research hotspots, which are necessary for energy storage and optimization of related renewable energy [4,5]. As a promising energy harvesting technology, triboelectric nanogenerator (TENG) has attracted considerable attention due to its sustainability and low cost [6,7], as it has been proven capable of harvesting energy from various sources, including human motion, wind, vibration and water currents, which makes it highly versatile in practical applications [8–12]. At the same time, the application directions of TENG are also very wide, covering smart phones, wearable devices, wireless sensor networks, fitness equipment and other fields [13]. It also has broad application prospects in environmental monitoring, intelligent transportation, smart home, medical and health fields [14,15].

Despite its well-established theoretical basis and significant advantages, the TENG faces several challenges that hinder its efficiency [16,17]. Furthermore, stability remains a significant problem in practical applications [18–20]. Therefore, in-depth research on the performance and mechanism of TENG is essential for promoting its practical application [21,22]. Scholars have explored and conducted experimental research, including

theoretical analysis and derivation, material selection and preparation, structure design and optimization, as well as performance testing and analysis, to address the challenges related to the TENG [23–27]. In addition to studying TENG's characteristics, developing a power management circuit that matches the output of TENG is crucial to improving its efficiency [28,29]. Hu et al. reported a simple and adjustable automatic spark switch circuit, which achieved energy accumulation and rapid release [30]. Cheng et al. proposed a dual-loop circuit, reducing the energy loss in the diode to 47.1% [31]. Zhang et al. demonstrated a universal power management circuit that achieved an efficiency of 80% in matching the impedance of a TENG [32]. A power management circuit can convert the TENG's alternating current (AC) output into a direct current (DC) output, which can power electronic devices or store energy in batteries or capacitors [33,34]. Maximizing harvested energy by increasing energy conversion efficiency is a significant challenge in TENG technology [35]. A suitable power management circuit can effectively enhance the TENG's output performance, playing a vital role in promoting its practical application.

In this paper, a power regulation circuit (PRC) suitable for TENG is proposed, which is composed of a first-stage valley-filling circuit and a second-stage switching step-down circuit, and its electrical performance is tested by a typical freestanding-mode TENG. Unlike common power management circuits that use switch circuits to reduce the duty cycle of the TENG, a PRC increases the conduction time of the TENG to increase the output charge and improve the energy utilization efficiency of the TENG. The experimental results show that adding the PRC increases the power supply time of the TENG in each cycle, thereby increasing the pulse number of the TENG output signal and the output charge is 1.6-fold higher than the initial value. Compared with the initial output signal, the charging rate of the output capacitor increases by 75%, improving the TENG's performance significantly. The stability of the PRC is further proved by frequency conversion charging experiments. At the same time, when the TENG supplies power to LEDs with a motion frequency of 2 Hz, the LEDs using the PRC flicker less than LEDs powered by direct rectification, the light is also more stable, further verifying the test results. The proposed PRC can efficiently utilize the output energy of the TENG, providing new insights into the storage and utilization of the TENG's energy.

2. Structure and Mechanism

Figure 1 presents a schematic diagram of a TENG and a PRC system, where Figure 1a illustrates the specific structure of the TENG. As the power supply segment of the PRC, the TENG is used to verify the applicability of the PRC for the TENG's power management and compared with the signal output after through the PRC. The TENG adopts a rotating freestanding mode, comprising a rotor, a shell and a shaft. The shell structure is made of an acrylic tube with a diameter of 94 mm, with six pairs of copper electrodes attached to its inner wall. The rotor is made of polylactide (PLA) material and uniformly inlaid with six pieces of fluorinated ethylene propylene (FEP) films, forming the power generation unit of the TENG. The TENG is driven by a rotating motor, and the output signals of the system are measured by a programmable electrometer and data acquisition system, which are processed and stored by LabVIEW software and computer. Figure 1b shows the schematic diagram of the PRC system, which consists of two-stage circuits. The first stage comprises a rectifier and a valley-filling circuit to increase the conduction time of the rectifier bridge during the TENG's unit motion cycle and enhance the initial output energy. The second-stage circuit steps down and stores the previous stage circuit to better match the output load. A PMOS transistor is used as a control switch, automatically turned on and off based on the magnitude of the first-stage output signal. To facilitate the experiment's debugging and component parameter determination, a PRC system was built on a breadboard, acting as a passive power management circuit directly connected to the TENG's output.

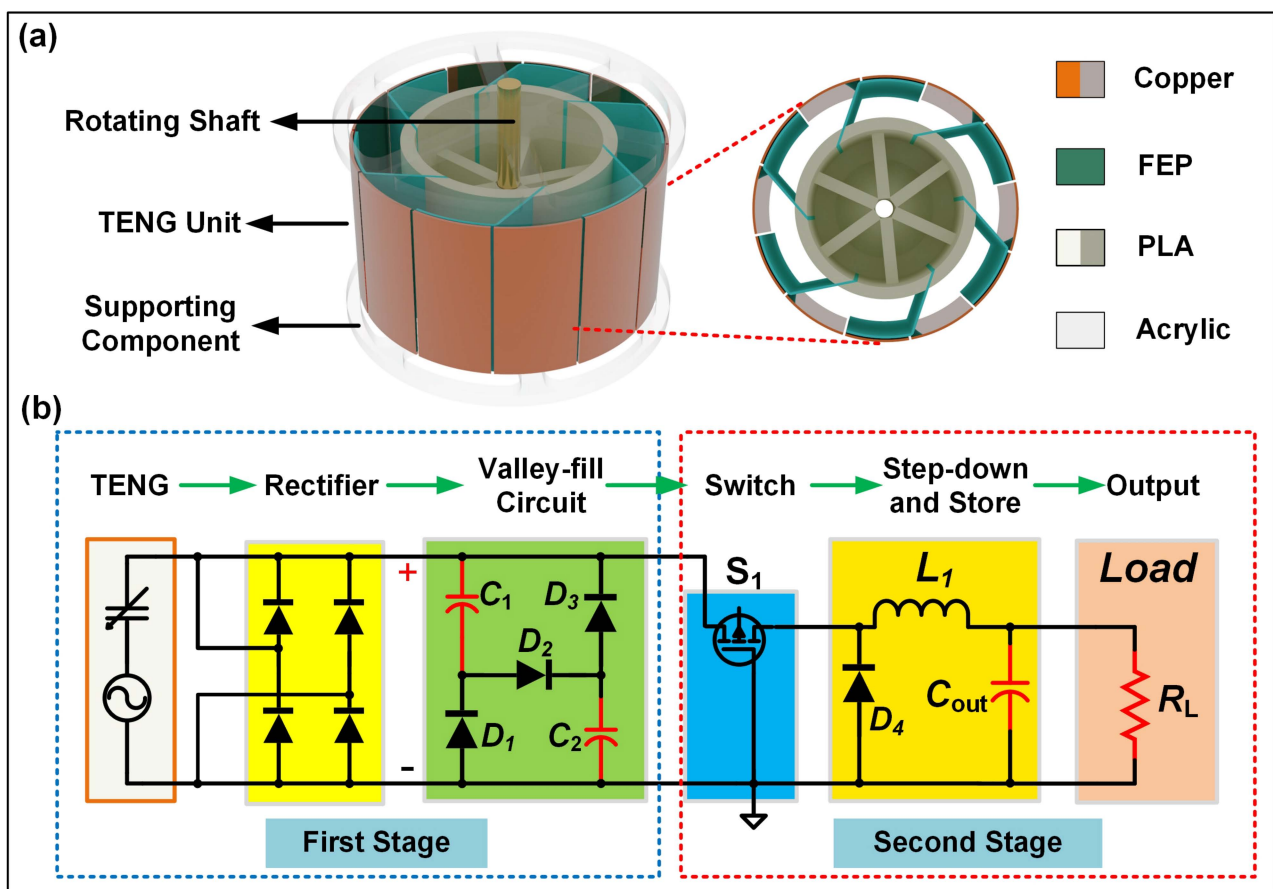


Figure 1. Design schematic diagram of the TENG and the PRC. (a) System structure of the TENG. (b) The circuit diagram of the PRC.

Figure 2 depicts the specific working principle of the TENG, which mainly comprises four processes. As presented in Figure 2a, according to the triboelectric sequence table, the FEP film surface easily gains electrons, resulting in a negative surface potential. Conversely, the copper electrode surface readily loses electrons, leading to a positive surface potential. In the initial state (Figure 2a(i)), the rotor remains stationary, and the FEP film is in full contact with copper electrode I. Consequently, contact electrification causes charge transfer, and both the copper electrode and the FEP film acquire equal amounts of positive and negative charges. When the FEP film is rotated to the state illustrated in Figure 2a(ii), it contacts both copper electrode I and copper electrode II, inducing electrostatic induction that drives electrons on electrode II towards electrode I, resulting in a secondary electrode under external load, and the current from electrode I to electrode II. As the rotor continues to move to the state displayed in Figure 2a(iii), the FEP film comes into complete contact with copper electrode II, and electrostatic equilibrium is reached, with no charge flowing. Subsequently, the rotor rotates to state iv (Figure 2a(iv)), under external load conditions, and a potential difference drives the generation of current in the opposite direction to the previous half-cycle, eventually returning to the initial state, initiating a new cycle. Therefore, continuous rotation of the TENG produces a continuous AC signal. Additionally, COMSOL was employed to simulate the electrostatic field, exhibiting the power generation mechanism of the TENG under different motion states (Figure 2b).

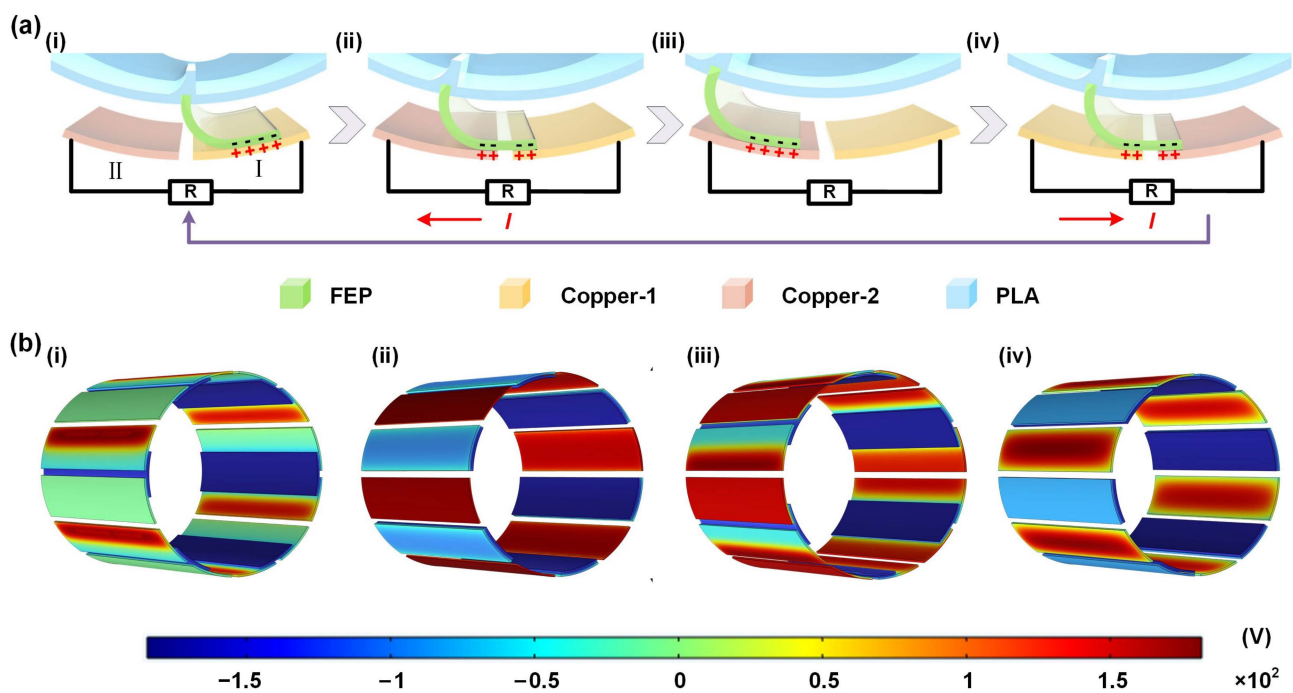


Figure 2. Principle analysis of the TENG: (a) The specific working principle of the TENG, (i–iv) the charge transfer relationship between the FEP film and the copper electrode when the TENG rotates; (b) (i–iv) simulation diagram of charge distribution in different states of the TENG.

Figure 3 illustrates the specific working process of the PRC. Figure 3a represents the first-stage circuit, which comprises a rectifier and a passive valley-filling circuit. To illustrate the functioning of the first-stage circuit, Figure 3b presents its detailed working principle. When the voltage of the TENG is high, the output current signal follows the path illustrated in Figure 3b(i). The current charges C_1 and C_2 , and D_2 conducts while D_1 and D_3 are cut off. In contrast, when the voltage is low, the capacitors C_1 and C_2 are discharged through D_1 and D_3 while D_2 is cut off, as shown in Figure 3b(ii). Meanwhile, when selecting a capacitor, it must be ensured that the values of C_1 and C_2 are equal, and in order to match the internal resistance of the TENG, the selection of the capacitor should not be too large. The selected capacitor value is $0.1 \mu\text{F}$. Furthermore, neglecting the voltage drop across the diodes, when the TENG output voltage attains V_m , the voltage drops across C_1 and C_2 are both $1/2 V_m$. Subsequently, when the output voltage of the TENG drops to $1/2 V_m$, the rectifier bridge diode is cut off. At this point, D_1 and D_3 conduct, and the two capacitors are connected in parallel to power the load. Compared to the basic rectifier circuit, the power supply after rectification needs to be higher than V_m to provide power to the external load. Therefore, as shown in Figure 3c, compared to the case of directly rectifying the output (Figure 3c(i)), the first-stage circuit increases the power supply time of the external load within one cycle, and due to the longer conduction time, only a small peak current is required to fulfill the power requirement within one cycle (Figure 3c(ii)). The second-stage output circuit, as illustrated in Figure 3d, comprises a PMOS switch and a step-down storage section. Figure 3e demonstrates the specific working process. Initially, when the output voltage V_i of the first stage reaches the threshold voltage of the switch S_1 , that is, when the source voltage of the PMOS transistor is 2 to 3 V higher than the gate voltage, the energy is transferred from the first-stage circuit to the second-stage circuit, and S_1 is passed through the change in the voltage is automatically turned on and off, and assists the second-stage circuit to realize the voltage reduction, realizing a regulation process of the passive switch. The output current powers the capacitor C_{out} and the load via the inductor L_1 , as depicted in Figure 3e(i). Conversely, when the voltage falls below V_i , the switch S_1 is tuned off, causing the energy stored in the inductor to be released to C_{out} and the load. At this point, D_4 is turned on, creating a closed loop, as shown in Figure 3e(ii). Ultimately, when the energy

stored in C_{out} reaches a certain threshold, it becomes capable of supplying stable power to the output load, as displayed in Figure 3e(iii). By employing the aforementioned two-stage circuits, the PRC system can accomplish the entire working process.

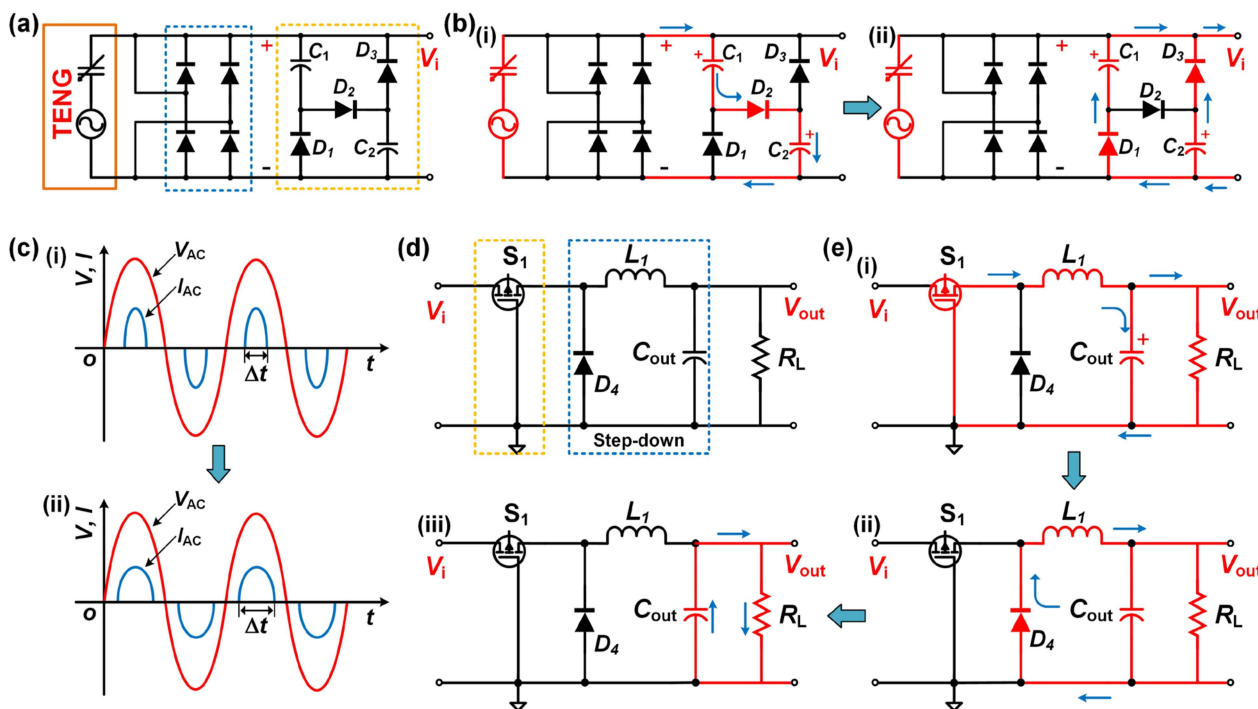


Figure 3. PRC-specific workflow: (a) the circuit diagram of the first stage in the PRC system; (b) the workflow of the first-stage circuit in the PRC, (i) series charging and (ii) parallel discharging of capacitors.; (c) the output mechanism diagram of the first-stage circuit in the PRC; (d) the circuit diagram of the second stage in the PRC system; (e) (i–iii) the workflow of the second-stage circuit within one cycle in the PRC.

3. Results and Discussion

3.1. Basic Output Performance

Figure 4 illustrates the fundamental performance tests of the TENG and the PRC. Specifically, Figure 4a(i–iii) exhibit the open-circuit voltage, short-circuit current, and transferred charge output signals of the TENG at different rotational speeds, respectively. Notably, the peak values of the open-circuit voltage and transferred charge remain nearly constant with increasing rotational frequency, whereas the short-circuit current gradually increases, having established the essential output performance and stable operating state of the TENG. Figure 4b(i,ii), respectively, demonstrate the short-circuit currents outputted by the TENG rectification and the TENG integrated with a first-stage circuit, at a consistent rotational speed of 120 rpm (unless stated otherwise, all subsequent experimental conditions were conducted at this rotational speed). The current pulse signals in Figure 4b(ii) appear to be more closely packed. To further elucidate the effect of the first-stage circuit in the PRC on the TENG output signal, Figure 4b(iii) compares the two sets of current signals in Figure 4b(i,ii) with amplification. It can be concluded that after the first-stage circuit, the number of pulse currents output by the TENG per unit time doubled, and the transferred charge amount increased by 60%. Although the peak current value slightly decreases, the accumulated energy output during the entire cycle shows a significant increase, which indicates that the first-stage circuit effectively increases the conduction time of the rectifier bridge diode of the TENG, leading to improved output power. It is worth noting that in the PRC system, the inductance L_1 plays a critical role in determining the circuit performance, particularly when the frequency of TENG motion is relatively high and the switch is rapidly turned on and off. To investigate this effect, experiments were carried out using different

inductance values, as shown in Figure 4c(i–iii). C_{out} with values of 10 μF , 22 μF , and 47 μF was used to test the charging time. Since the motion frequency of the TENG itself is not high, μH level inductance values are chosen. The capacitance charging curves show that the charging rate of C_{out} increases with an increasing inductance value. However, when the value of L_1 exceeds 330 μH , the delay caused by inductance becomes more significant, leading to a reduction in the charging rate. Based on our results, the optimal value of L_1 is between 150 μH and 330 μH .

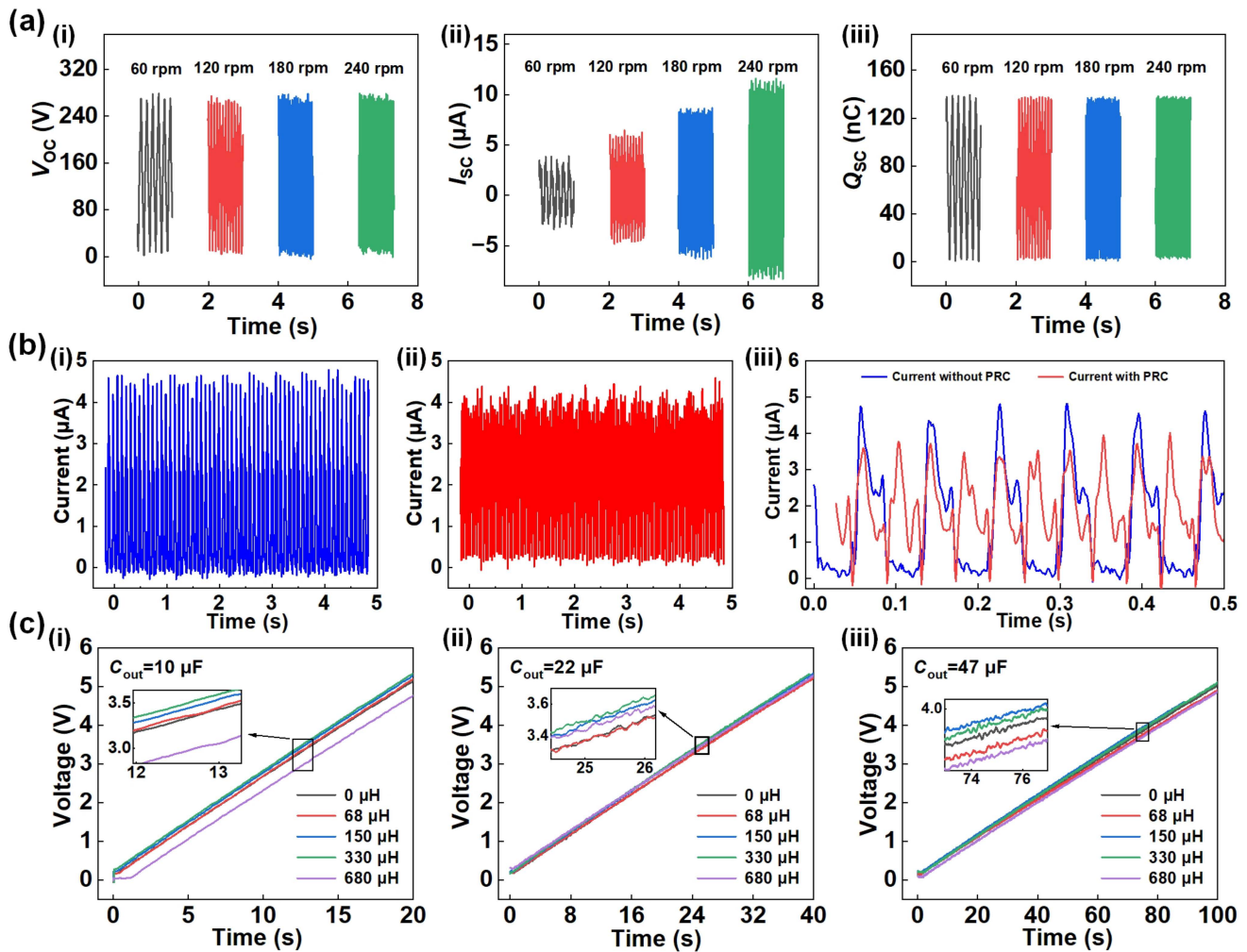


Figure 4. Basic output characteristics of the TENG and the PRC. (a) (i–iii) The original signals of voltage, current and charge of the TENG at different frequencies; (b) (i) short-circuit current output by direct rectification and (ii) by the PRC of the TENG, (iii) amplification of the current signal for comparison; (c) (i–iii) influence of different inductance values on charging characteristics of output capacitor.

3.2. Demonstration of the PRC

Once the basic principles and parameters of the PRC system are determined, Figure 5 presents the final output performance analysis of the PRC system, along with comparative experiments and application demonstrations. Figure 5a shows the load charging characteristic curves for different C_{out} of 10 μF , 22 μF , and 47 μF , indicating that the internal resistance of the TENG should be considered when choosing the load. If the C_{out} is insufficiently large, the load voltage will fluctuate, leading to poor load-bearing capacity. Moreover, when the capacitance of C_{out} remains constant, the charging speed of C_{out} will be faster with a larger load. Comparative experiments were conducted as shown in Figure 5b(i,ii), where capacitors were charged under two different output conditions, one with the PRC system and the other without it. The results demonstrate that the charging rate of capacitors increased by 75% when the capacitor is charged to 5 V with the PRC system included. In

addition, the charging time is significantly reduced with the inclusion of the PRC system. In order to verify the stability of the PRC system, Figure 5c presents a bar chart of the charging time of three groups of output capacitors charged to 5 V under different TENG motion frequencies. The charging time ratios of the three groups of capacitors are also tested at different frequencies using 3 Hz as the reference frequency, as shown in the curve in Figure 5c, the three curves almost coincide and can be fitted into one curve, indicating that the charging time varies proportionally with the motion frequency, and the entire circuit system is very stable. Finally, Figure 5d demonstrates the actual application capability of the PRC circuit through an experimental demonstration. Figure 5d(i) shows the testing system diagram, and the power supply of LEDs under two output modes, direct rectification and PRC output, is tested at a TENG speed of 120 rpm. The experimental findings indicate that when the LEDs are connected to the PRC (as illustrated in Figure 5d(i) and Video S1 in the Supplementary Materials), the flashing phenomenon is reduced and the overall lighting process becomes more stable. These demonstration results are consistent with the test data, thus confirming that the PRC can enhance the output efficiency of the TENG and improve the output stability.

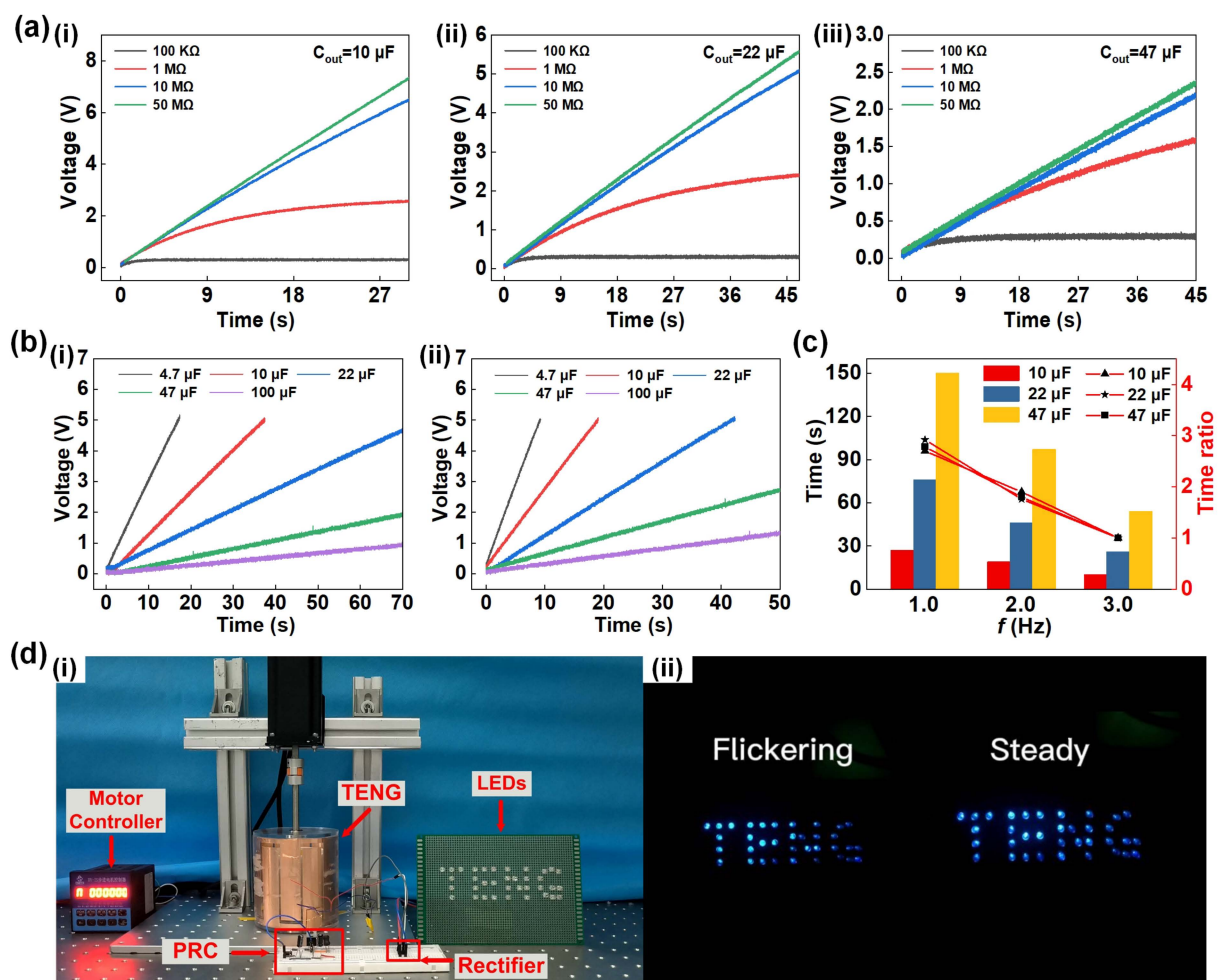


Figure 5. The output performance test and application demonstration of the PRC. (a) (i–iii) Curves of the charging voltage and the charging rate of C_{out} under different loads; (b) comparison experiment of output capacitor charging (i) with PRC and (ii) without the PRC; (c) the relationship between frequency and charging time; (d) (i) experimental test physical diagram and (ii) application demonstration of the TENG powering LEDs in two output modes.

4. Conclusions

In summary, the PRC system increases the power supply time of the TENG in each cycle, thereby increasing the number of pulses in the TENG output current signal. As a result, the total output energy per unit cycle increases, and compared to the initial output signal, the charging rate of the output capacitor increases by 75% after the PRC is added, improving the output efficiency of the TENG significantly. The PRC consists of a first-stage valley-filling circuit and a second-stage switching step-down circuit. The circuit performance was tested by a rotation-type freestanding-mode TENG. The frequency conversion charging experiment further demonstrated the stability of the PRC. At the same time, when the TENG supplies power to the LEDs at 120 rpm, the LEDs using the PRC flicker less and emit more stable light than the LEDs supplied by direct rectification, further validating the test results. The PRC proposed in this study can more effectively harvest and utilize the TENG's energy, which has a certain promoting effect on the storage and utilization of the output energy of the TENG.

Supplementary Materials: The following are available online at <https://www.mdpi.com/article/10.3390/s23104912/s1>, Video S1: Demonstration of lighting LEDs by the TENG with and without a PRC.

Author Contributions: Conceptualization, W.L and X.C.; software, W.L.; investigation, W.L., B.L., S.H. and X.C.; resources, X.C.; writing—original draft preparation, W.L., B.L., S.H. and X.C.; writing—review and editing, X.C.; supervision, X.C. All authors have read and agreed to the published version of the manuscript.

Funding: This research received no external funding.

Institutional Review Board Statement: Not applicable.

Informed Consent Statement: Informed consent was obtained from all subjects involved in this study.

Data Availability Statement: Not applicable.

Conflicts of Interest: The authors declare no conflict of interest.

Nomenclature

TENG	Triboelectric Nanogenerator
PRC	Power Regulation Circuit
PLA	Poly lactide
FEP	Fluorinated Ethylene Propylene
PMOS	Positive channel Metal Oxide Semiconductor
C_1, C_1	Capacitance of the first-stage circuit
D_1, D_2, D_3, D_4	Diode
L_1	Inductance
C_{out}	Output Capacitance
R_L	Load
V_i	Input Voltage
V_{out}	Output Voltage

References

1. Le, C.D.; Vo, C.P.; Vu, D.L.; Nguyen, T.H.; Ahn, K.K. Water electrification based triboelectric nanogenerator integrated harmonic oscillator for waste mechanical energy harvesting. *Energy Convers. Manag.* **2022**, *251*, 115014. [[CrossRef](#)]
2. Niu, S.M.; Wang, X.F.; Yi, F.; Zhou, Y.S.; Wang, Z.L. A universal self-charging system driven by random biomechanical energy for sustainable operation of mobile electronics. *Nat. Commun.* **2015**, *6*, 8975. [[CrossRef](#)] [[PubMed](#)]
3. Elsanadidy, E.; Mosa, I.M.; Luo, D.; Xiao, X.; Chen, J.; Wang, Z.L.; Rusling, J.F. Advances in Triboelectric Nanogenerators for Self-powered Neuromodulation. *Adv. Funct. Mater.* **2023**, *33*, 2211177. [[CrossRef](#)]
4. Curto, D.; Favuzza, S.; Franzitta, V.; Guercio, A.; Amparo Navarro Navia, M.; Telaretti, E.; Zizzo, G. Grid Stability Improvement Using Synthetic Inertia by Battery Energy Storage Systems in Small Islands. *Energy* **2022**, *254*, 124456. [[CrossRef](#)]
5. Harada, K.; Yabe, K.; Takami, H.; Goto, A.; Sato, Y.; Hayashi, Y. Two-step approach for quasi-optimization of energy storage and transportation at renewable energy site. *Renew. Energy* **2023**, *211*, 846–858. [[CrossRef](#)]

6. Zhang, X.S.; Gao, Q.; Gao, Q.; Yu, X.; Cheng, T.H.; Wang, Z.L. Triboelectric Rotary Motion Sensor for Industrial-Grade Speed and Angle Monitoring. *Sensors* **2021**, *21*, 1713. [[CrossRef](#)]
7. Wang, Z.L. Triboelectric nanogenerators as new energy technology and self-powered sensors—Principles, problems and perspectives. *Faraday Discuss.* **2014**, *176*, 447–458. [[CrossRef](#)]
8. Kim, W.G.; Kim, D.W.; Tcho, I.W.; Kim, J.K.; Kim, M.S.; Choi, Y.K. Triboelectric Nanogenerator: Structure, Mechanism, and Applications. *ACS Nano* **2021**, *15*, 258–287. [[CrossRef](#)]
9. Wang, Z.L.; Jiang, T.; Xu, L. Toward the blue energy dream by triboelectric nanogenerator networks. *Nano Energy* **2017**, *39*, 9–23. [[CrossRef](#)]
10. Pathak, M.; Kumar, R. Synchronous Pre-biasing of Triboelectric Nanogenerator for Enhanced Energy Extraction. *IEEE Trans. Power Electron.* **2022**, *37*, 11552–11566. [[CrossRef](#)]
11. Zhang, B.S.; Li, W.B.; Ge, J.W.; Chen, C.G.; Yu, X.; Wang, Z.L.; Cheng, T.H. Single-material-substrated triboelectric-electromagnetic hybrid generator for self-powered multifunctional sensing in intelligent greenhouse. *Nano Res.* **2023**, *16*, 3149–3155. [[CrossRef](#)]
12. Zhao, B.; Zhao, K.; Wang, X.C.; Liang, J.R.; Chen, Z.Y. Series Synchronized Triple Bias-Flip Circuit: Maximizing the Usage of a Single Storage Capacitor for Piezoelectric Energy Harvesting Enhancement. *IEEE Trans. Power Electron.* **2021**, *36*, 6787–6796. [[CrossRef](#)]
13. Fang, L.; Zheng, Q.W.; Hou, W.C.; Gu, J.Y.; Zheng, L. A self-powered tilt angle sensor for tall buildings based on the coupling of multiple triboelectric nanogenerator units. *Sens. Actuators A Phys.* **2023**, *349*, 114015. [[CrossRef](#)]
14. Zhang, B.S.; Zhang, S.; Li, W.B.; Gao, Q.; Zhao, D.; Wang, Z.L.; Cheng, T.H. Self-Powered Sensing for Smart Agriculture by Electromagnetic–Triboelectric Hybrid Generator. *ACS Nano* **2021**, *15*, 20278–20286. [[CrossRef](#)] [[PubMed](#)]
15. Wang, Z.L. Self-Powered Nanotech. *Sci. Am.* **2008**, *298*, 82–87. [[CrossRef](#)] [[PubMed](#)]
16. Li, Y.H.; Yu, J.R.; Wei, Y.C.; Wang, Y.F.; Feng, Z.Y.; Cheng, L.Q.; Huo, Z.W.; Lei, Y.Q.; Sun, Q.J. Recent Progress in Self-Powered Wireless Sensors and Systems Based on TENG. *Sensors* **2023**, *23*, 1329. [[CrossRef](#)] [[PubMed](#)]
17. Duan, Q.S.; Peng, W.Q.; He, J.X.; Zhang, Z.J.; Wu, Z.C.; Zhang, Y.; Wang, S.F.; Nie, S.X. Rational Design of Advanced Triboelectric Materials for Energy Harvesting and Emerging Applications. *Small Methods* **2023**, *7*, 2201251. [[CrossRef](#)]
18. Wang, H.M.; Xu, L.; Bai, Y.; Wang, Z.L. Pumping up the charge density of a triboelectric nanogenerator by charge-shuttling. *Nat. Commun.* **2020**, *11*, 4203. [[CrossRef](#)]
19. Cheng, G.; Lin, Z.H.; Lin, L.; Du, Z.L.; Wang, Z.L. Pulsed Nanogenerator with Huge Instantaneous Output Power Density. *ACS Nano* **2013**, *7*, 7383–7391. [[CrossRef](#)]
20. Wang, Z.L.; Song, J.H. Piezoelectric Nanogenerators Based on Zinc Oxide Nanowire Arrays. *Science* **2006**, *312*, 242–246. [[CrossRef](#)]
21. Xi, F.; Pang, Y.; Liu, G.; Wang, S.; Li, W.; Zhang, C.; Wang, Z.L. Self-powered intelligent buoy system by water wave energy for sustainable and autonomous wireless sensing and data transmission. *Nano Energy* **2019**, *61*, 1–9. [[CrossRef](#)]
22. Zargari, S.; Daie Koozehkanani, Z.; Veladi, H.; Sobhi, J.; Rezania, A. A new Mylar-based triboelectric energy harvester with an innovative design for mechanical energy harvesting applications. *Energy Convers. Manag.* **2021**, *244*, 114489. [[CrossRef](#)]
23. Cao, X.L.; Xiong, Y.; Sun, J.; Xie, X.Y.; Sun, Q.J.; Wang, Z.L. Multidiscipline Applications of Triboelectric Nanogenerators for the Intelligent Era of Internet of Things. *Nano-Micro Lett.* **2022**, *15*, 14. [[CrossRef](#)] [[PubMed](#)]
24. He, W.C.; Shan, C.C.; Fu, S.K.; Wu, H.Y.; Wang, J.; Mu, Q.J.; Li, G.; Hu, C.G. Large Harvested Energy by Self-Excited Liquid Suspension Triboelectric Nanogenerator with Optimized Charge Transportation Behavior. *Adv. Mater.* **2023**, *35*, 2209657. [[CrossRef](#)] [[PubMed](#)]
25. Rasel, M.S.; Maharjan, P.; Park, J.Y. Hand clapping inspired integrated multilayer hybrid nanogenerator as a wearable and universal power source for portable electronics. *Nano Energy* **2019**, *63*, 103816. [[CrossRef](#)]
26. Wang, Z.; Tang, Q.; Shan, C.C.; Du, Y.; He, W.C.; Fu, S.K.; Li, G.; Liu, A.P.; Liu, W.L.; Hu, C.G. Giant performance improvement of triboelectric nanogenerator systems achieved by matched inductor design. *Energy Environ. Sci.* **2021**, *14*, 6627–6637. [[CrossRef](#)]
27. Xu, L.Q.; Xuan, W.P.; Chen, J.K.; Zhang, C.; Tang, Y.Z.; Huang, X.W.; Li, W.J.; Jin, H.; Dong, S.R.; Yin, W.L.; et al. Fully self-powered instantaneous wireless humidity sensing system based on triboelectric nanogenerator. *Nano Energy* **2021**, *83*, 105814. [[CrossRef](#)]
28. Fan, F.-R.; Tian, Z.-Q.; Wang, Z.L. Flexible triboelectric generator. *Nano Energy* **2012**, *1*, 328–334. [[CrossRef](#)]
29. Zhang, H.M.; Marty, F.; Xia, X.; Zi, Y.L.; Bourouina, T.; Galayko, D.; Basset, P. Employing a MEMS plasma switch for conditioning high-voltage kinetic energy harvesters. *Nat. Commun.* **2020**, *11*, 3221. [[CrossRef](#)]
30. Wang, Z.; Liu, W.L.; He, W.C.; Guo, H.Y.; Long, L.; Xi, Y.; Wang, X.; Liu, A.P.; Hu, C.G. Ultrahigh Electricity Generation from Low-Frequency Mechanical Energy by Efficient Energy Management. *Joule* **2021**, *5*, 441–455. [[CrossRef](#)]
31. Zhang, Z.H.; Gu, G.Q.; Zhang, W.H.; Gu, G.X.; Shang, W.Y.; Liu, Y.; Cheng, G.; Du, Z. Double loops power management circuit of pulsed triboelectric nanogenerator with enhanced efficiency at low operating voltage and its application in self-powered flue gas monitoring system. *Nano Energy* **2023**, *110*, 108360. [[CrossRef](#)]
32. Xi, F.; Pang, Y.; Li, W.; Jiang, T.; Zhang, L.; Guo, T.; Liu, G.; Zhang, C.; Wang, Z.L. Universal power management strategy for triboelectric nanogenerator. *Nano Energy* **2017**, *37*, 168–176. [[CrossRef](#)]
33. Jiang, D.W.; Lian, M.Y.; Xu, M.J.; Sun, Q.; Xu, B.B.; Thabet, H.K.; El-Bahy, S.M.; Ibrahim, M.M.; Huang, M.N.; Guo, Z.H. Advances in triboelectric nanogenerator technology—Applications in self-powered sensors, Internet of things, biomedicine, and blue energy. *Adv. Compos. Hybrid Mater.* **2023**, *6*, 57. [[CrossRef](#)]

34. Wu, H.; Wang, S.; Wang, Z.K.; Zi, Y.L. Achieving ultrahigh instantaneous power density of 10 MW/m² by leveraging the opposite-charge-enhanced transistor-like triboelectric nanogenerator (OCT-TENG). *Nat. Commun.* **2021**, *12*, 5470. [[CrossRef](#)]
35. Zhu, P.C.; Zhang, B.S.; Wang, H.Y.; Wu, Y.H.; Cao, H.J.; He, L.B.; Li, C.Y.; Luo, X.P.; Li, X.; Mao, Y.C. 3D printed triboelectric nanogenerator as self-powered human-machine interactive sensor for breathing-based language expression. *Nano Res.* **2022**, *15*, 5098–5104. [[CrossRef](#)]

Disclaimer/Publisher’s Note: The statements, opinions and data contained in all publications are solely those of the individual author(s) and contributor(s) and not of MDPI and/or the editor(s). MDPI and/or the editor(s) disclaim responsibility for any injury to people or property resulting from any ideas, methods, instructions or products referred to in the content.